Spatially resolved measurements of grain size effects on the shock and spall response of quasi-Taylor wave loaded pure copper

G. Whiteman, G. D. Owen, J. De'Ath, D. J. Chapman, D. E. Eakins, J. G. Turner, and J. C. F. Millett

Citation: Journal of Applied Physics **122**, 035106 (2017); doi: 10.1063/1.4986626
View online: http://dx.doi.org/10.1063/1.4986626
View Table of Contents: http://aip.scitation.org/toc/jap/122/3
Published by the American Institute of Physics

Spatially resolved measurements of grain size effects on the shock and spall response of quasi-Taylor wave loaded pure copper

G. Whiteman,[1] G. D. Owen,[1] J. De'Ath,[1] D. J. Chapman,[2] D. E. Eakins,[2] J. G. Turner,[1] and J. C. F. Millett[1]
[1]*AWE, Aldermaston, Reading RG7 4PR, United Kingdom*
[2]*Institute of Shock Physics, Blackett Laboratory, Imperial College London, London SW7 2AZ, United Kingdom*

(Received 6 June 2017; accepted 7 July 2017; published online 21 July 2017)

Quasi-Taylor wave loaded plate impact experiments have been used to study the effects of bulk grain size on the shock and spall response of pure copper samples. Using line-Velocity Interferometry System for Any Reflector velocimetry, an increased particle velocity dispersion was measured for larger bulk grain size samples resulting in lower mean peak particle velocities and a lower reload velocity following spall. Spall voids were located in a surface layer of similarly sized grains for both bulk grain size materials tested. The spall strength was observed to vary with the tensile strain-rate but was unaffected by the bulk grain size. Post-mortem studies of voids in samples showed narrow void planes for the small bulk grain size materials and a larger spread of voids in the larger bulk grain size materials consistent with the free surface particle velocity data and observed particle velocity dispersion. [http://dx.doi.org/10.1063/1.4986626]

I. INTRODUCTION

The measurement and modelling of dynamic tensile failure under shock loading, often termed spall, is of persistent interest and importance to a myriad of industrial and research institutions. The ability to correctly predict a structure's response to impacts and explosive loads is required for both civilian and military applications including the design of vehicles, buildings, and satellites. Necessarily the materials used to build such structures are limited by real world practicalities and are therefore typically heterogeneous at the mesoscale (e.g., grain-scale) level. These local heterogeneities will affect the bulk scale loading response of a structure which may or may not result in significant consequences for the intended purpose. As such it is clearly necessary to study these effects and develop a framework of understanding which would allow both phenomenological assessments of microstructural effects and accurate predictions which can inform the design process.

Much of the experimental shock research which can be found in the literature focuses on point (or spatially averaged) measurements of response to determine quantities such as the Hugoniot elastic limit (HEL) and spall strength. The laser spot size of diagnostics such as Heterodyne Velocimetry (HetV)[1] and the Velocity Interferometry System for Any Reflector (VISAR)[2] determines the spatial resolution of the velocity measurements. Spot sizes are typically of the order 100 μm–1 mm diameter which might encompass 1 to 100 typically sized grains at the measurement surface and will record the combined effects of the wave interactions with the full material structure through the target thickness. The variation of measured particle velocities could be statistically analysed from multiple small spot size point measurements on single or repeat experiments, however, spatially resolved velocimetry offers a more direct and useable statistical basis for the measurement of these behaviours on individual experiments. Line-imaging VISAR,[3,4] or simply line-VISAR (LV), is a such spatially and temporally resolved diagnostic. It has been used in shock research since its inception, however, its use at high resolution for quantitative studies of mesoscale phenomena is relatively uncommon[5–9] as the fielding and data analysis required to ensure real phenomena are being investigated is not trivial. When applied carefully, it can therefore be used in the development of crystal plasticity and multiscale models which might ultimately be used for the accurate prediction of the bulk structural loading problem.

In this research, we have chosen to address the measurement of the dynamic effects of mesoscale structures by applying line-VISAR to measure the shock response of polycrystalline pure copper. We have decided to focus on the variations of the free surface particle velocity and the incipient spall response of quasi-Taylor (or "triangular") wave loaded copper with two significantly different bulk grain sizes. It is known that the progression of spall in shocked materials varies with different planar loading profiles, for example whether a square pulse or a Taylor wave is applied.[10,11] Such loading differences will alter the width of the spall plane and the stress and strain-rate history seen by the material in tension. Spall behaviour will also be affected by the material defects generated by the first compression wave,[12] by local defect structure (e.g., grain boundary distribution) in the failure region,[13,14] and is likely to be sensitive to the shock wave's deviation from an ideal planar form, i.e., the "roughness" or particle velocity dispersion (PVD) of the shock wave.[7,15] The effects of PVD and grain boundary distribution are generally coupled in spall experiments where the grain structure in the bulk of the sample creates locally distributed wave structures which subsequently interact to create a region of tension within the same grain structure. Due to material availability in this research (see Sec. II), we were able to decouple these effects to some degree by having different bulk grain sizes in different samples but a very

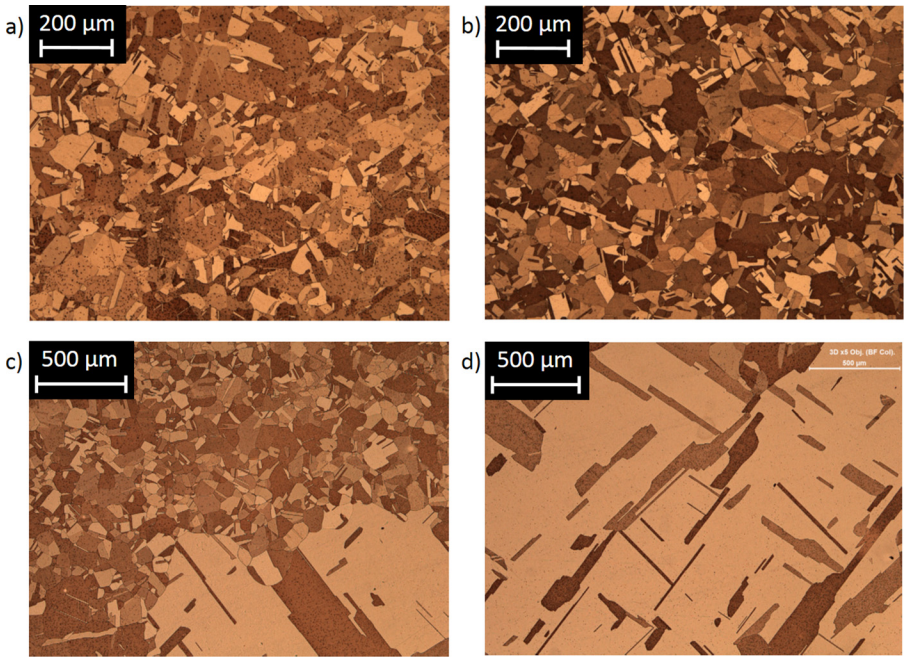

FIG. 1. Optical microscopy images for (a) SGCu sample in the surface layer, (b) SGCu sample in the bulk material, (c) LGCu sample in the boundary between the surface and bulk, and (d) LGCu sample in the bulk material.

similar grain size distribution in the region of tension for each sample.

II. MATERIALS

The material tested in this research was oxygen free high conductivity (OFHC) copper, 99.997 wt. % pure, sourced from *Aurubis* as a 12.7 mm thick plate stock in the half hard condition. This material is of similar specification, with almost identical chemistry and mechanical properties to that used in previous work by Escobedo *et al.*[14] and Gray *et al.*[16] allowing close comparison to that data. The copper was subsequently annealed in two batches at 600 °C for 1 h and 850 °C for 4 h. This produced grain sizes with an approximate log-normal distribution with mean bulk grain sizes (including annealing twins) of ∼30 μm and ∼150 μm with underlying grain sizes (i.e., not including twins) of ∼60 μm and of the order of 1 mm for the small and large bulk grain size materials, respectively. The small and large grain copper materials are respectively referred to as SGCu and LGCu throughout this paper. As the initially supplied plate material had been cold rolled, once it had been annealed the LGCu material contained an approximately 1.5 mm thick surface layer of smaller grains (∼45 μm mean size including annealing twins). Figure 1 shows example optical microscopy of the initial materials. The results indicated that both materials had a largely equiaxed grain structure with a number of annealing twins. Figure 1 highlights the variation in the initial bulk grain structures and the surface layer effect. The similar grain size surface layer for both materials was utilised in these experiments to ensure that the region of tension and therefore spallation occurred in a similar grain structure for both materials. This is discussed further in Sec. IV.

By applying a triangular loading pulse in these experiments, we were able to place the plane of spallation near the rear surface of the samples. This in turn allowed us to ensure that the spall planes for both bulk grain size materials tested occurred in locations within the samples with similar grain sizes. This meant that the grain boundary length in the tensile region was largely unchanged and only the PVD, which is affected by the bulk grain structure, was altered between samples of SGCu and LGCu. The schematic diagram in Fig. 2 highlights the material structure, spall plane location, and the effect of the bulk grain structure on the PVD. PVD, which can be quantified as the ratio of the standard deviation to the mean of multiple measured particle velocities of a sample, was measured in these experiments at the rear free surface of the samples. As such the surface layer will have

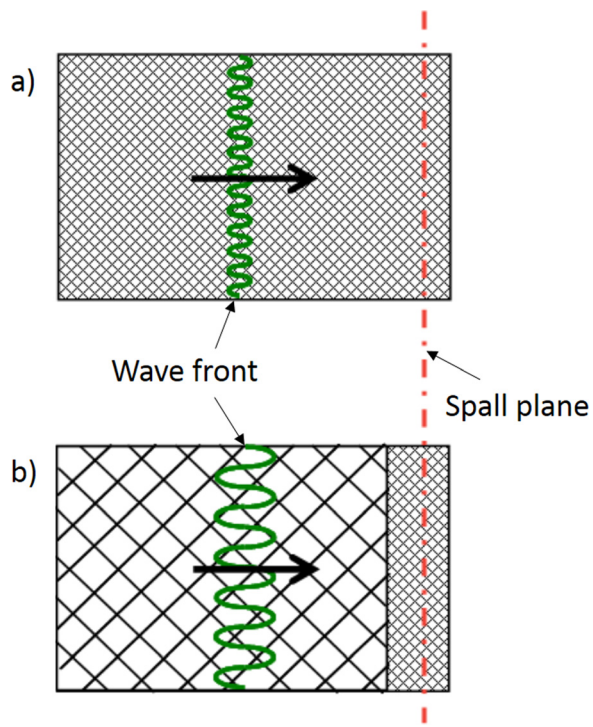

FIG. 2. Schematic representation of copper material grain structures and shock fronts in this research for (a) SGCu and (b) LGCu samples.

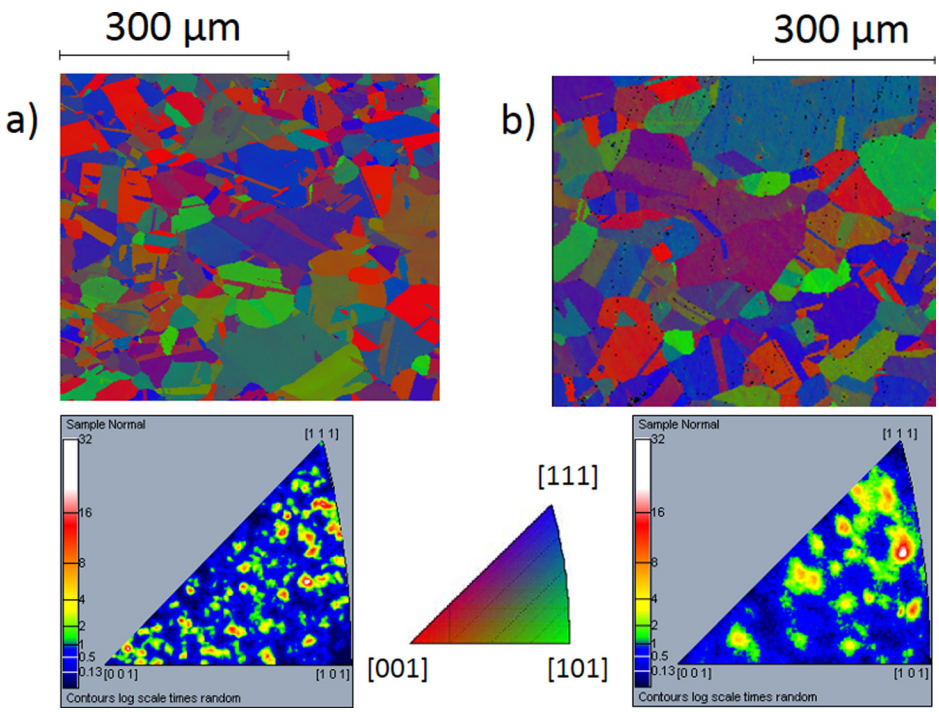

FIG. 3. EBSD orientation maps of surface layers for (a) SGCu sample and (b) LGCu sample. EBSD images are shown with their respective inverse pole figures.

had an additional complicating effect on the dispersion measured at the rear free surface of the large bulk grain size material.

The sample microstructures were also investigated *via* electron back scatter diffraction (EBSD). Examples for the surface layer are shown in Fig. 3. Analysis of EBSD images (for both bulk and surface layers) showed a weak crystallographic texture.

Results of density and sound speed measurements undertaken on the initial materials are shown in Table I. The sound speeds generally agree with literature values although were slightly larger and more variable for LGCu, presumably due to the lower number of grains in the sample thickness.

III. LINE-VISAR

The line-VISAR is a velocity interferometry diagnostic based on the classic VISAR system,[2] which uses moving interference fringes caused by the motion of a reflecting surface to determine surface velocity. In line-VISAR, the photodetectors are specifically replaced by a streak camera to streak a slit image of the fringes with time thus producing a temporally and spatially resolved velocity record which can be used for lines from a few tens of microns up to several millimetres in length for microseconds of recording time.

In these experiments, a single streak camera (Optronis SC-51 coupled to a Spectral Instruments SI800 CCD detector) line-VISAR with the interferometer set in the Mach-Zehnder configuration, was used. High resolution and significant line length were desirable in these experiments which are competing factors and the set up used was considered the best compromise. The line length was set to $\sim$3 mm on the sample surface with a total record length of $\sim$2.5 μs to ensure recording of the full 1D dynamic event and at least 0.5 μs of static data before surface motion. The fringe size was set to 20 mm^{-1} across the full line length to achieve spatial resolutions, measured prior to each experiment, of at least 75 μm for a $\leq$5% velocity accuracy. Much smaller features were also observable but with >5% error. The slit width was measured to be $\sim$15 pixels which is equivalent to $\sim$35 μm on the sample surface and $\sim$20 ns in the streaked dynamic experiments. The line-VISAR and analysis methods used in this research are described in more detail in a recent article.[17] The analysis method applied is a 1D continuous wavelet transform (CWT) analysis with issues such as streak camera distortion and fixed pattern noise accounted for.

IV. EXPERIMENTS

Parallel-plate impact experiments were performed on a 100 mm bore single stage compressed helium driven gas-gun located at the Institute of Shock Physics, Imperial College London. The impact and diagnostic configuration for these experiments is shown in Fig. 4. Each target consisted of two nominally 10 mm thick, 45 mm diameter copper samples, four small PMMA windows, and eight piezoelectric pins mounted flush to the front face of a copper retaining plate. The copper samples were mounted within the 12 mm thick

TABLE I. Details of initial material characterisation.

Material	Density (g/cm^3)	c_L – Longitudinal sound speed (mm/μs)	c_S - Shear sound speed (mm/μs)	Mean bulk grain size, including twins (μm)
SGCu	8.92 ± 0.01	4.77 ± 0.01	2.32 ± 0.01	30
LGCu	8.92 ± 0.01	4.83 ± 0.02	2.34 ± 0.05	150

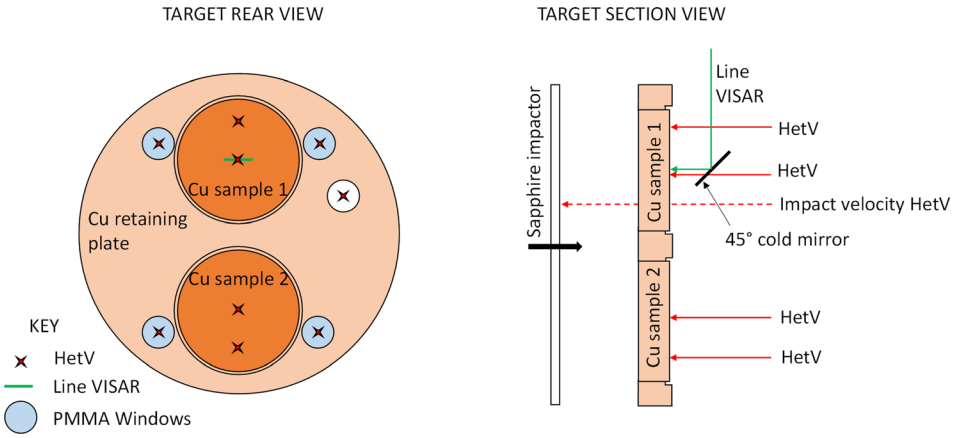

FIG. 4. Schematic layouts for these experiments of (a) impact configuration and (b) diagnostic configuration.

retaining plate in holes with ∼50 μm clearance on radius. A 4 mm deep counter bore on the rear of the plate was used to allow the epoxy adhesive to hold the samples in place.

The motion of the target rear-surface was diagnosed using line-VISAR. The line-VISAR was fielded *via* a 45° angled front surface cold-mirror centrally located on one of the samples on each experiment. Impact tilt and timing in these experiments were measured using a combination of HetV[1] through the PMMA windows and the piezoelectric pins. HetV is a point velocimetry diagnostic which in these experiments, employing collimating lens probes mounted in alignment gimbals, was mounted ∼10 mm from the sample surfaces and produced effective spot sizes on the reflecting surfaces of ∼200 μm diameter. Two channels of HetV were fielded on the rear surfaces of each copper sample, one ∼13 mm from the sample edge and one at the sample centre (through the cold-mirror on the line-VISAR sample of each experiment). A final channel of HetV was used to measure the impact velocity through a hole in the target. The approximate locations of the HetV surface measurements and the mirror used to return the line-VISAR light out from the target vacuum enclosure of the gas gun are shown in Fig. 4(b).

The impact face of the full target was lapped such that it was flat to <2 μm and each individual sample was flat to <1 μm. Additionally, the rear surface of each sample was polished to a mirror finish to reduce the effects of laser speckle, allowing tight optical fringe spacing (20 mm^{-1}) on the line-VISAR diagnostic which in turn improves spatial resolution. The targets were impacted by thin (∼1 mm and ∼3 mm thick) z-cut sapphire flyer plates mounted to a polycarbonate sabot. The sapphire flyer plates were ground such that they were parallel to ≤3 μm and flat to ≤10 μm across each sample. Table II shows the full details of each experiment.

As shown in the table, experiments 1, 2, and 5 were undertaken with the thin sapphire flyer plate at approximately the same impact velocity, ∼260 m/s. This produced an impact stress at the loading surface of ∼5.3 GPa and a short pulse triangular wave at the rear recording surface with a peak velocity of ∼195 m/s (equivalent to ∼3.6 GPa). We also chose to investigate the effect of increasing the pulse duration while still retaining a triangular wave loading at the spall plane in experiments 3 and 4. This was achieved by increasing the thickness of the sapphire flyer to ∼3 mm and reducing the impact velocity. As the release front from the rear of the impactor catches up with the shock front deeper into the sample for the thicker impactor, the reduction of impact velocity was required to attempt to match the peak stress at the spall plane between the "short pulse" and "long pulse" configurations. A simulated rear free surface velocity history is shown in Fig. 5 to highlight the key features of a shock and spall trace and the intended difference between the short and long triangular pulse experiments. These 1D simulations were undertaken using the AWE Lagrangian hydrocode CORVUS[18] with a mesh size of 2 μm. Strength and spall were incorporated using the Preston Tonks Wallace (PTW)[19] and Johnson spall[20] models, respectively.

Of interest in these particular experiments is the spall behaviour (e.g., spall strength, the reload signal, and the developed microstructure) of the different grain size samples. The spall strength is a convenient parameter to define and compare the material's resistance to applied dynamic tension. There are various definitions of spall strength, most of which attribute a single value based on an assumed perfectly planar failure in an isotropic material. In most cases,

TABLE II. Details of the plate impact experiments. Note: the first sample in each experiment featured the Line-VISAR (LV). No tilt or velocimetry data was recorded on Shot 4.

Shot #	1st Sample (LV): Material and thickness ± 0.005 (mm)	2nd Sample: Material and thickness ± 0.005 (mm)	Sapphire Impactor thickness ± 0.002 (mm)	Impact tilt ± 0.05 (mrads)	Impact velocity (m/s)
1: Short pulse	SGCu 9.87	SGCu 9.92	1.001	0.19	259.9 ± 0.5
2: Short pulse	LGCu 9.94	SGCu 9.96	0.989	0.31	259.6 ± 0.5
3: Long pulse	SGCu 10.01	LGCu 10.01	2.997	0.54	149.5 ± 0.5
4: Long pulse	SGCu 9.98	SGCu 9.96	3.001	…	170.0 ± 10.0
5: Short pulse	LGCu 9.98	LGCu 10.00	0.991	0.31	266.5 ± 0.5

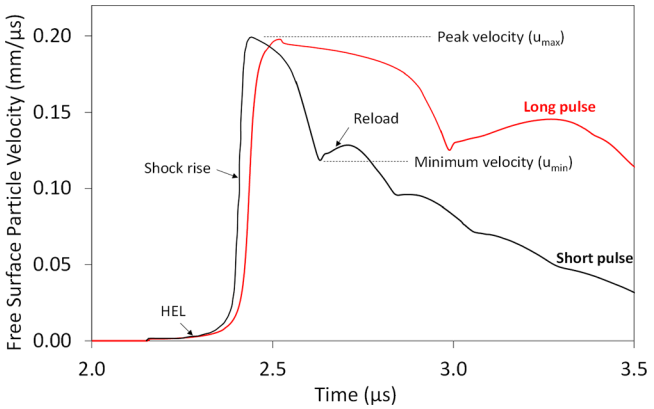

FIG. 5. Simulated rear free surface velocity history for quasi-Taylor wave loaded spall experiments.

the definition of spall strength (σ_S) is proportional to the pull-back signal (Δu_{fs}) which is the magnitude of the difference between the measured peak free surface velocity (u_{max}) and the minimum in the free surface velocity (u_{min}), as shown in Fig. 5. As such, spall strength is most readily associated with the initial tensile stress which causes significant nucleation of voids rather than subsequent growth and coalescence of the voids. Here we define spall strength in Eq. (1) following the recommendation of Kanel[21] for an elasto-plastic material as

$$\sigma_S = \rho_0 c_L \Delta u_{fs}/(1 + c_L/c_0), \tag{1}$$

where ρ_0 is the material density and c_L and c_0 are the ambient pressure longitudinal wave speed and bulk sound speed, respectively. This form of the equation is applicable to triangular compression pulses where the reload pulse travels at the longitudinal sound velocity independent of its steepness.

Note that Shots 3 and 4 in this series fired slower than the intended 190 m/s impact velocity such that the peak stresses in the spall region were ~2.8 and 3.2 GPa respectively although it is not considered that this would make a significant difference to the spall behaviour and mechanisms observed. For Shot 4, no velocimetry was recorded such that only the recovered microstructure is included in this work. Metallography of the recovered samples was considered to be a secondary diagnostic in these experiments. Due to the significant quantity of hardware located behind the samples, it would not be feasible to recover them without some post shot damage. However, by use of the shock impedance matched retaining copper plate and ensuring some areas of the samples would not directly impact the hardware, it was considered that post shot metallurgy would still provide data regarding void plane location, approximate void sizes, and the extent of coalescence.

V. RESULTS: LINE-VISAR

An example line-VISAR derived 2D spatially resolved velocity record and 3D velocity plot are shown in Fig. 6 from Shot 3 on the SGCu material.

The raw streak camera data was corrected for issues such as streak camera distortion and fixed pattern noise and analysed as discussed in Philpott *et al.*[17] Figure 6(a) shows the analysed record converted from pixels to real time and velocity values. The static run-in can be seen at the beginning of the record although the low (~3 m/s) elastic precursor, which lasts for ~250 ns before the shock rise, is not easily discernible in the image. At approximately 1 μs, there is an abrupt rise to the peak free surface velocity as the shock arrives, then the pullback signal and subsequent oscillations corresponding to wave reverberations through the spall layer. It can often be easier to visualize the line-VISAR data using 3D surface plots [Fig. 6(b)] where images are plotted in velocity, distance, and time space for every pixel of the camera's CCD (equivalent to ~2 μm per pixel on the sample surface).

3D surface plots comparing the different bulk grain size materials for short pulse experiments are shown in Fig. 7. Here, significant spatial variation of velocity is apparent in the measured response across the surfaces. This variation, which appears quasi-periodic in nature is the greatest for the larger bulk grain size materials [e.g., Fig. 7(b)] although is still significant, with a higher frequency, for the small grain size material [e.g., Fig. 7(a)].

The grain size at the recording surface for this data (~45 μm) is lower than the stated system resolution (~75 μm) although the line-VISAR system is capable of

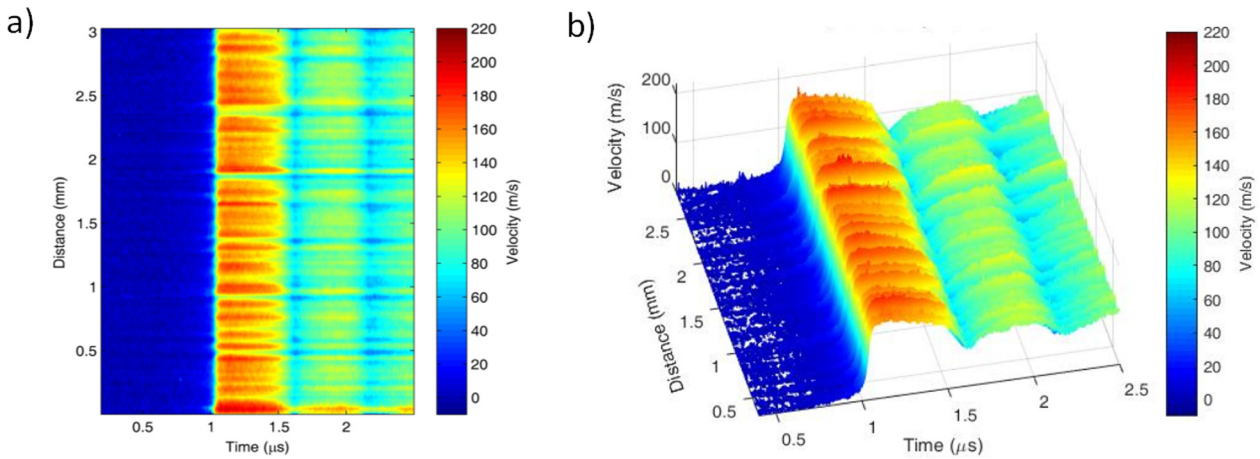

FIG. 6. Line-VISAR velocity record for Shot3, SGCu material in (a) 2D plot and (b) 3D surface plot.

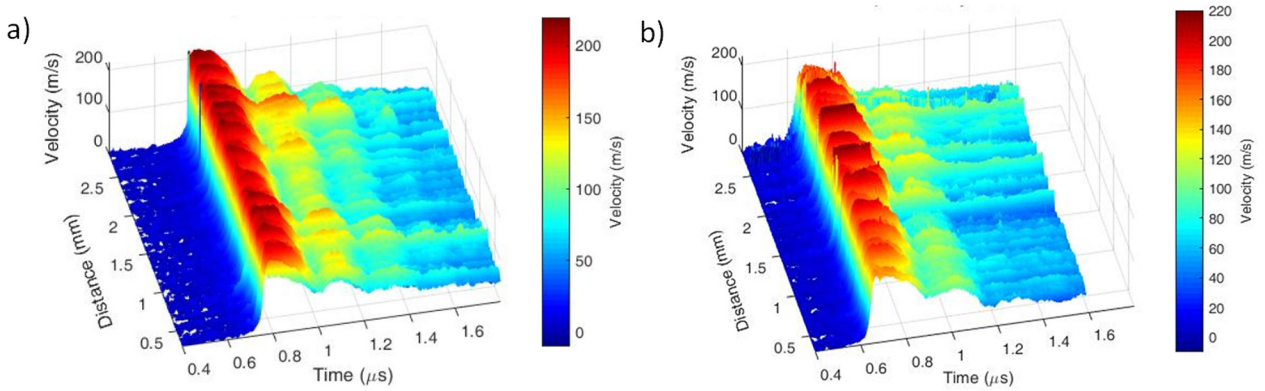

FIG. 7. 3D surface plots of velocity data for (a) SGCu material, Shot 1 and (b) LGCu material, Shot 2.

measuring much smaller spatial features (<10 μm) with an increased velocity uncertainty. This suggests that the variations such as the quasi-periodic nature observed in Fig. 7, which appear to be on the scale of hundreds of microns, are real surface behaviour. Line-outs of the line-VISAR velocity data at certain times have also been taken to produce velocity distributions. Example distributions using 5 m/s bins through the peak free surface velocity for Shots 1 and 2 are shown in Fig. 8. It can be seen that the free surface particle velocities approximate to normal distributions over the 3 mm line lengths even with the quasi-periodic nature noted previously. Despite near identical loading conditions, Fig. 8 also indicates that the mean particle velocities achieved are lower for the LGCu material although the maximum velocity achieved is the same. This observation seems physically reasonable as no obvious mechanism would increase the maximum velocity achieved such that a greater dispersion of particle velocities caused by the larger bulk grain structure will therefore naturally reduce the mean velocity.

To account for the system resolution, we have chosen to analyse the data further by taking a series of non-overlapping spatial averages. In Fig. 9 are a series of non-overlapping 100 μm averages across the 3 mm line for all of the experiments. Also included in the figure are the (total pixel) mean and the standard deviation of the line-VISAR data as well as a single HetV data set from the same experiment (the

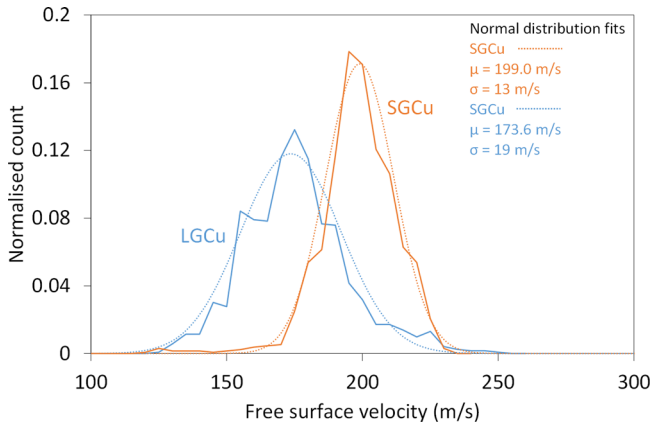

FIG. 8. Distribution of particle velocities for SGCu (Shot 1) and LGCu (Shot 2) materials line-VISAR data taken through the peak of the triangular wave.

remainder of which are shown in Sec. VI). The ~200 μm diameter HetV spots would have encompassed approximately ten times the surface area compared to the 100 μm × 35 μm line-VISAR averages. It is also noted that for Shot 5 some unphysical velocity spikes were recorded in portions of the data. A finer spatial resolution was targeted in this experiment by increasing the fringe density to ~28 mm^{-1}. This equates to a wavelength of ~36 μm, close to the operational wavelength of the interferometer set-up which resulted in the analysis routine becoming unstable and unable to correctly unwrap the velocity information across the full width of the line. Approximately 1.7 mm of data was obtained which was of similar quality to the other experiments but was interspersed by regions of significant velocity spikes. These have been removed from the 100 μm velocity average analysis for clarity. Further development of the analysis may enable more of the data to be unwrapped in the future.

Figure 9 shows that the velocity variation around the mean is clearly significant in all cases. The maximum to minimum variations are ~20 m/s for the SGCu material and ~60 m/s for the LGCu material. Inspection of the 100 μm average data reveals that there is correlation between adjacent data sets signifying real surface behaviour rather than system or analysis noise. The standard deviation of the measured free surface particle velocities shown in Fig. 9 displays a distinctive peak during the shock rise where relatively small variations in wave arrival times will result in large departures from the mean. The measured variations of the shock arrival time were ~30 ns and ~80 ns across the full extent of the line for the SGCu and LGCu samples, respectively. These peaks are similar to those predicted in discrete element model simulations of shocked polycrystalline copper[15] and observed experimentally in shock loaded tungsten.[7] The standard deviation in the early baseline data was approximately 3 m/s in all cases indicating the systematic error in the system. The standard deviations in the dynamic data after the shock rise display slowly varying levels of ~13 m/s for the small grain material and ~19 m/s for the large (although it does vary more significantly for Shot 5 where unphysical velocity spikes were more prevalent). These results suggest a significant particle velocity dispersion in all cases which is more severe for the large bulk grain

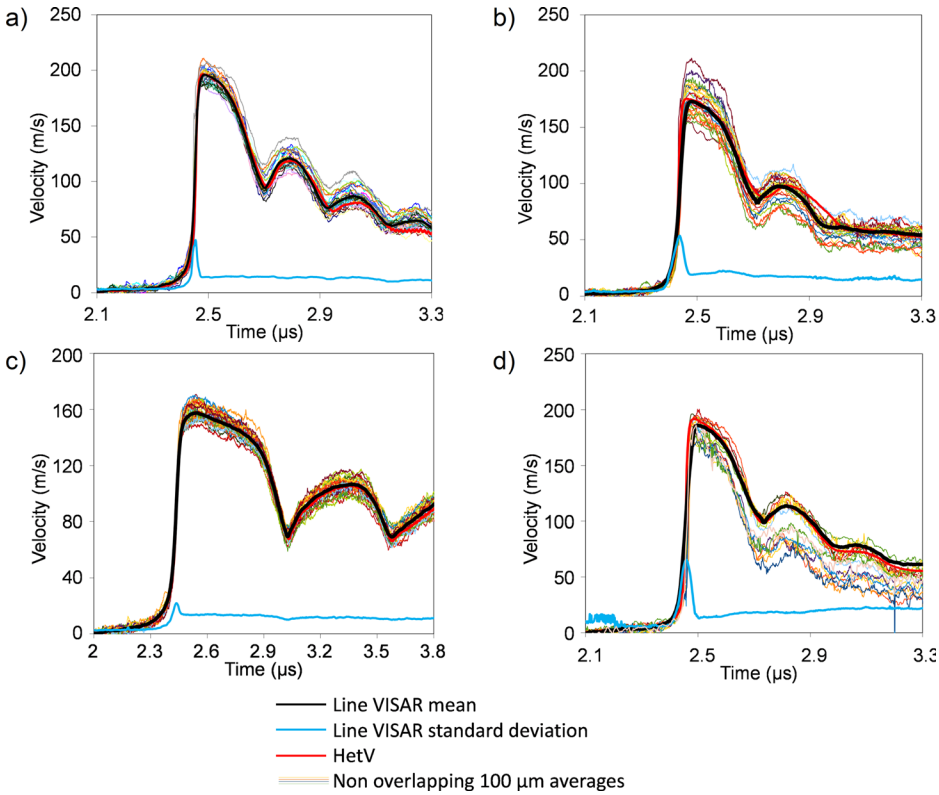

FIG. 9. Non-overlapping 100 μm averages of line-VISAR data for (a) Shot 1: short pulse, SGCu material, (b) Shot 2: Short pulse, LGCu material, (c) Shot 3: Long pulse, SGCu material, and (d) Shot 5: Short pulse, LGCu material. A single HetV record, the line-VISAR total pixel mean, and the line-VISAR total pixel standard deviation are shown in bold red, black, and blue lines respectively for each data set.

material although mean line-VISAR data for both materials as shown in Fig. 9 is closely consistent with the HetV data.

VI. RESULTS: HetV

In Fig. 10, the measured free surface HetV profiles for these experiments are displayed aligned to impact time [Figs. 10(a) and 10(c)] and the first free surface minimum [Figs. 10(b) and 10(d)]. Figures 10(a) and 10(b) show the data for the SGCu material and Figs. 10(c) and 10(d) show the data for the LGCu material along with a single short and long pulse data set for the SGCu material for comparison.

Figure 10(a) shows the consistency of behaviour of the SGCu samples from multiple HetV measurements on multiple samples. In contrast, the pairs of probes on each LGCu sample seen in Fig. 10(c) exhibit clear differences, ~4–6 m/s between probes on the same samples for both short and long pulse experiments. It is notable that the peak free surface velocity achieved is also significantly different between the large and small grain size materials as observed in the

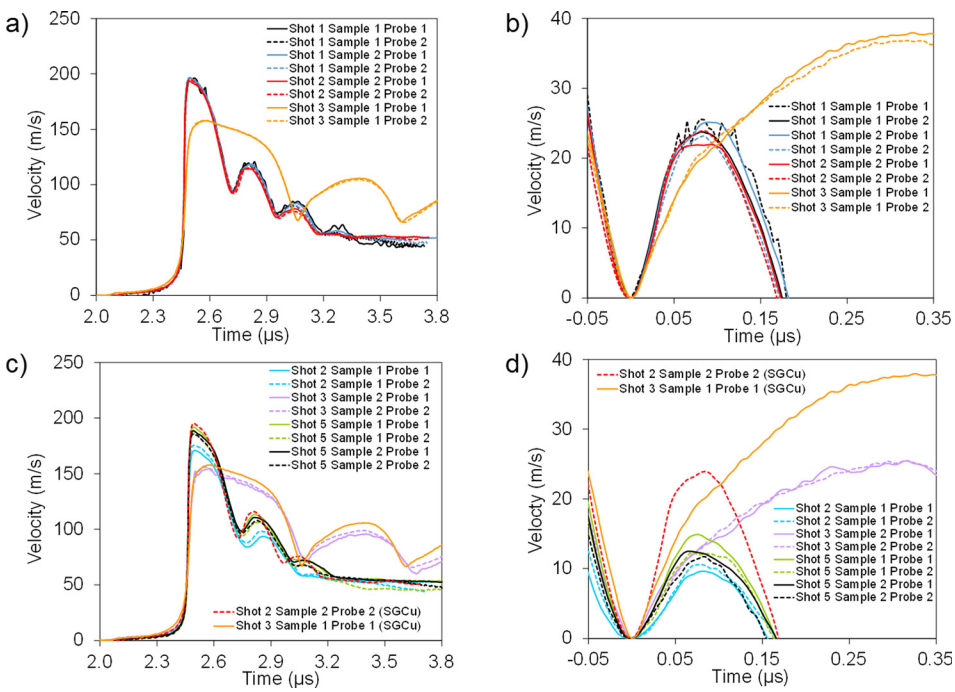

FIG. 10. HetV free surface velocity history data for (a) SGCu material aligned to impact time = 0 μs; (b) SGCu material aligned to the first free surface minimum; (c) LGCu material aligned to impact time = 0 μs (compared to small grain size sample); and (d) LGCu material aligned to the first free surface minimum.

line-VISAR data. For Shot 2, the LGCu material reached a peak of ~20 m/s lower than the SGCu sample on the same target despite the identical impact conditions and near identical target thicknesses. This wave dispersion effect reducing the average peak particle velocity was offset on Shot 5, featuring two LGCu samples, by increasing the impact velocity. It can be seen that a more comparable peak free surface velocity was achieved (compared to SGCu samples) in that case. Figure 10(c) also shows that for the short pulse experiments, the reverberating waves in the incipiently spalled scab reduce to very little after the first reload in the LGCu material suggesting that the large bulk grains have the effect of dispersing the waves and therefore are likely to create a wider, more incipient spall plane.

The longer pulse experiment (Shot 3) did not reach the same peak velocity as previously discussed, however by alignment of all the records to the first free surface minimum [Figs. 10(b) and 10(d)], we are able to compare the reload signal behaviours. This portion of the data is where the effects of void growth and coalescence are most evident. Figure 10(b) shows that for both loading pulses, the initial reload after spall is similar but for the longer pulse experiment the velocity then grows more slowly. The fast initial reload suggests consistent void nucleation for the SGCu material but for the shorter loading pulse experiments there is then limited time and less kinetic energy in the thinner spall scab to allow significant growth and coalescence of voids. In Fig. 10(d), the reload acceleration and the peak velocity are lower for the LGCu samples and also significantly more variable, suggesting fewer and more widely spaced voids.

VII. RESULTS: SPALL STRENGTH

Spall strengths have been calculated for both the HetV and the line-VISAR data using Eq. (1) and are plotted in Fig. 11, as a function of the tensile strain-rate ($\dot{\varepsilon}$). The tensile strain-rate is calculated immediately prior to spallation using

$$\dot{\varepsilon} = (\dot{u}_{fs}/2c_0), \tag{2}$$

where $\dot{u}_{fs}$ is the maximum gradient of the free surface velocity before failure. For these data, the error in the strain-rate is omitted for clarity in Fig. 10 but is calculated to be approximately $\pm 0.002\ \mu s^{-1}$. The spall strength has been calculated at every pixel for the line-VISAR data and the mean is presented with the standard deviation as the error. The spall strength error for the HetV data, also omitted in the figure for clarity, is approximately 1%.

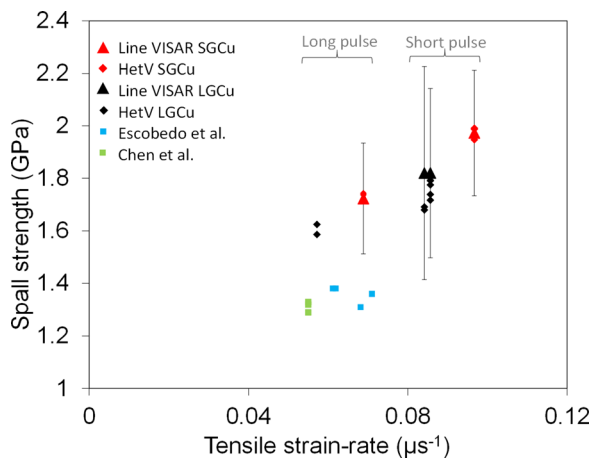

FIG. 11. Spall strength *versus* tensile strain-rate for all experiments.

The relationship between spall strength and tensile strain-rate is shown in Fig. 11 alongside data from the literature.[13,14] The figure indicates a gradual increase of spall strength with tensile strain-rate for both bulk grain size materials and both pulse lengths tested in these experiments. Lower average tensile strain-rates are observed for lower peak free surface velocities, i.e., for the long pulse experiments and for the LGCu material in general where a greater particle velocity spread results in a lower peak velocity for the same loading. There is a larger spread of spall strength determined for the LGCu materials observed in the multiple HetV data points and the standard deviation on the line-VISAR data. The variation of spall strength for the SGCu material determined from the line-VISAR data is less than for the LGCu material but is also not insignificant in agreement with the line-VISAR analyses shown in Fig. 9. The trend in the spall strength (σ_S) data implies that for the copper materials tested the nucleation of voids is predominantly dependent on the tensile strain-rate, and that the sensitivity to the structure/spatial variation in the tensile wave arising from the different bulk grain structure is small. It is the case however that the bulk grain size affects the observed error in σ_S. This is expected due to the change in the roughness of the loading and release waves affecting void locations within the spall plane and therefore the subsequently observed wave profiles at the rear free surface.

Data from similar copper materials from the literature[13,14] is also included in Fig. 11 for comparison. These data were produced for square wave loaded samples with a variety of grain sizes from ~30 μm to 400 μm. They show no obvious effects of grain size on pullback velocity at low impact stresses and result in lower spall strength than the observed trend in the current research. This highlights some of the important differences between square and triangular wave loading, where spall plane widths and total damage volume induced (for a similar peak free surface velocity) will be different. For example in Escobedo *et al.*,[14] the observed width of the incipient spall planes produced were >0.5 mm while for this research they were <0.2 mm. The increased "plane" width will probe a larger volume of material allowing more of the weakest potential void nucleation sites to be activated. In Chen *et al.*,[13] where peak free surface velocities were similar to the current research, the authors observed significant damage leading to mostly complete spall scab separation. The mostly incipient spall we observe, particularly for the short pulse loading, is shown in more detail in Sec. VIII.

VIII. RESULTS: MICROSCOPY

As expected, due to the large amount of hardware behind the targets in these experiments and the relative proximity of the spall planes to the rear surface, there were

limited areas suitable for metallographic study. A series of optical and EBSD images were however taken in areas deemed far enough away from obvious impact features which has enabled some qualitative assessment of void properties to support conclusions based on the dynamic velocimetry data. EBSD imaging in areas where the voids had not coalesced significantly showed that voids preferentially formed at grain boundaries but that the special boundary types corresponding to $\sum 1$ low angle ($<5°$) and $\sum 3$ ($\sim 60° \langle 111 \rangle$ misorientation) were more resistant to void formation as was also found in a previous study.[14] Example optical microscopy images of the recovered void planes for the four experimental conditions are shown in Fig. 12. Figures 12(a) and 12(b) show the void planes for the SGCu material and Figs. 12(c) and 12(d) show the void planes for the LGCu material. Note that the void planes for the long pulse length experiments were both significantly coalesced and the example images shown [Figs. 12(b) and 12(d)] have been chosen in areas where full coalescence was not achieved in order to highlight some of the underlying void locations.

Figure 12 indicates that in general, the local void plane widths are narrow in these experiments. Lower magnification images (not shown) showed that the overall positions of the spall planes varied by hundreds of micrometers across the samples due to the roughness of the shock profiles and the local grain structures. The locations of the spall "planes" with respect to the free surfaces measured from recovered samples on these experiments were 0.43 ± 0.04 mm, 1.03 ± 0.04 mm, 0.48 ± 0.08 mm, and 1.15 ± 0.1 mm for the SGCu short pulse, SGCu long pulse, LGCu short pulse, and LGCu long pulse experiments, respectively. Fig. 12(a) shows a SGCu short pulse experiment in which a large number of closely spaced voids are observed. The voids are of the order of $\sim 20\,\mu$m in diameter and are not heavily coalesced. In contrast for the SGCu long pulse experiment, Fig. 12(b) shows that while there was a similar number and distribution of voids initially, these have coalesced significantly. Across the sample, there were large areas of almost complete separation of the spall scab. In Fig. 12(c), for the LGCu short pulse experiment there are noticeably fewer, more isolated voids than seen in the SGCu although those present are of approximately the same size, $\sim 20\,\mu$m in diameter. Compared to the short pulse SGCu samples, the voids are a similar distance from the free surface but more widely spread. In Fig. 12(d), the LGCu long pulse experiment shows a largely coalesced void distribution. Across the whole sample, there was still significant void coalescence but it was generally less extreme than for the equivalent SGCu samples. Qualitatively, the coalesced voids appear to be made up of larger voids which would be consistent with the more widely spaced initial void structure allowing more significant void growth of individual voids before coalescence occurred.

In summary it appears that for the short pulse loading there is insufficient time and less kinetic energy in the thinner spall scab for significant coalescence to occur and hence void growth dominates the damage behaviour. For the SGCu material, the less dispersed tensile region means that a significant number of voids can be formed, whereas for the greater particle velocity dispersion of the LGCu materials less voids overall are formed. For the longer pulse loading, the initial void nucleation and growth behaviour are likely to be very similar to the short pulse experiments (despite minor differences in the tensile strain-rate). These voids will then grow and coalesce quickly for the SGCu material but will slowly grow larger before coalescence for the LGCu material.

IX. DISCUSSION

Perfectly planar shocks are not possible in real materials, where mesoscale structures such as grains with different crystallographic orientations must lead to local anisotropies. Experimental quantification and simulation of these effects is challenging although the roughness of shocks, quantified

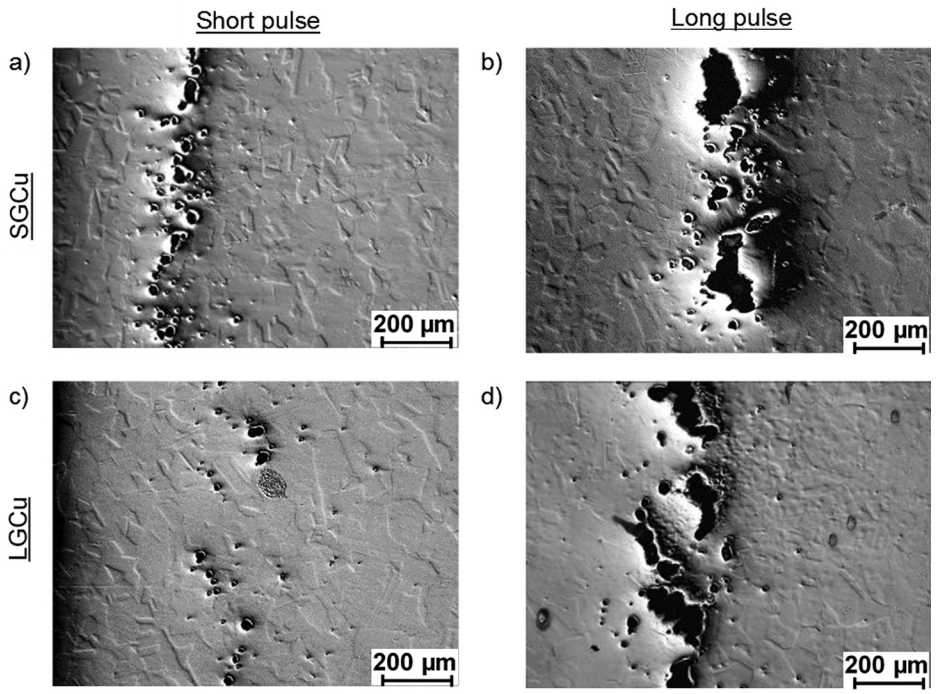

FIG. 12. Example optical microscopy images of spall planes for (a) SGCu, short pulse, (b) SGCu, long pulse, (c) LGCu, short pulse, and (d) LGCu, long pulse.

by particle velocity dispersion (PVD), has been shown to affect the macroscopic properties of dynamic shear and spall strength.[22–25] The results presented in this paper provide further experimental evidence of the presence of these locally distributed wave fronts, a quantification of the associated particle velocity fluctuations, and the resultant variations in spall behaviour.

In this research, two significantly different bulk grain sizes of copper have been used to alter the dispersion of the wave fronts in the shocked samples. The line-VISAR data presented shows that for all experiments, the variation in the magnitude and timing of the measured particle velocity along the 3 mm measurement line was significant. The standard deviation (σ_{fs}) of the line-VISAR velocities shows a peak at the mid-point of the shock rise which then relaxes to a non-zero level of ~13 m/s and ~19 m/s for the SGCu and LGCu materials, respectively. These values are consistent with those observed for similar line-VISAR experimental studies on shocked tantalum[8] and tungsten.[7] If we assume a Gaussian distribution of the wave front position, then 99.7% of the free surface positions will lie $\pm 3\sigma$ from the mean. For these experiments, this equates to the free surface location variation after approximately 2 μs of motion being $\sim\pm 60\,\mu$m and $\pm 110\,\mu$m from the mean for the SGCu and LGCu materials, respectively. It is expected that this free surface measurement will be about twice the internal material value.[15,22] Normalised PVD can be defined as

$$PVD_n = \bar{\sigma}_{fs}/\bar{u}_{fs}, \tag{3}$$

where $\overline{\sigma}_{fs}$ is the average standard deviation of the free surface line-VISAR data from the beginning of the shock rise to the record end and $\overline{u}_{fs}$ is the mean free surface velocity over the same period. Assessing PVD_n for the SGCu material results in values of 0.153 and 0.114 (Shots 1 and 3, respectively) and for the LGCu material it equals 0.245 and 0.298 (Shots 2 and 5, respectively). The SGCu data is similar to the value of 0.09 determined *via* interference contrast measurements from the free surface of shocked targets on another copper material (of unspecified grain structure) at a similar rear surface shock stress of ~3.2 GPa.[22] Similarly, discrete element simulations of shock propagation in polycrystalline copper shocked to ~3.4 GPa, carried out by Case and Horie,[15] yielded a normalised PVD of 0.05. These simulations produce a low but similar scale comparison with our experimental data however they only consisted of 143 grains with a mean diameter of 14 μm (with a log-normal grain size distribution) in a 160 μm × 160 μm simulated target. As such, larger scale simulations with grain and targets sizes of similar scale to these current experiments would give a more complete comparison.

Previous research has also suggested that PVD will increase both with distance travelled through a sample[15,26] and with average free surface velocity.[15,27] In the current research, it would therefore be expected that the thick samples have accentuated the PVD growth even though the peak free surface velocities are similar. It would seem physically reasonable to assume that PVD growth will not increase indefinitely throughout a thick sample as an approximate equilibrium should set in due to micro-stress relaxation from the most forward positions in a shock front travelling laterally in the sample. From these current experiments, no evidence based comment can be made as to the growth rates of the PVD although it is likely to be a function of the grain size itself. It should also be noted that the application of triangular loading pulses may also affect the PVD growth as the rarefaction will have caught and interacted with the shock front within the sample. The values of σ_{fs} however do not noticeably change during the spallation part of the signals suggesting that wave interaction effects are minimal in this case.

It is important to highlight that the quantification of PVD discussed in this research is not entirely the result of the bulk grain-size. The complicating effect of the finer grained surface layer in the large bulk grain size material should also be appreciated. When the shock wave moves from the large bulk grain size material into the surface layer the dispersion will begin to reduce, the extent of which has not been investigated. As such, the PVD measured at the rear surface is less than would be seen in the bulk and is a superposition of the local grain size effects and the remaining effects from the bulk material. At the spall plane itself this is probably more complex as the interacting parts of the wave have travelled different distances through the surface layer such that dispersion of both will be affected to different degrees.

The HetV velocimetry data, shown in Fig. 10, also showed variation for the LGCu data suggestive of PVD. Due to spot size resolution we observed no variation for the SGCu material. No variations were also reported for any grain sizes tested in previous research[13,14] on spalled copper although the larger diameter spot sizes (~1 mm) would likely have smoothed out any variable behaviours in their larger grain material data.

The wave interactions and resultant spallation in materials must necessarily be dependent on the particle velocity dispersion present. In many experiments, the grain structure responsible for the variation of particle velocities is also the medium in which failure occurs meaning effects such as the total grain boundary length in the spallation zone is changed along with the dispersion. Previous research has shown contradictory evidence between the grain size in the region of tension and pullback velocity suggesting either a Hall–Petch type relationship,[28] its inverse (with spall strength increasing with grain size)[29,30] or no observable effect.[14] In this research, we were able to remove this complication and decouple the effect of grain size in the region of tension to ensure that the effects of the dispersion were addressed independently. It was seen that the bulk grain size did not significantly affect the spall strength (i.e., the tension at void nucleation) in these experiments but did noticeably influence the void locations. After the void nucleation, subsequent growth and coalescence differences were observed in the recovered microstructures and the reload velocimetry data. As observed in comparison of Figs. 12(a) and 12(c), the larger particle velocity dispersion creates fewer, more isolated voids which subsequently produce a lower and more variable reload signal at the rear free surface [see Figs. 9(b) and 10(d)].

Previous researchers investigated the square pulse loaded spall of a similar small grain sized copper and compared it with a larger grain size material.[14] In their research, the authors found that the initial reload was similar for all grain sizes but that the signal slowed for smaller grains giving an overall lower reload. In the current data we observe the opposite as the reload is slower for the larger bulk grain material. In the former example, the explanation given is a change from void growth dominated damage behaviour (in the small grain material) to coalescence dominated in the larger grain samples. In that case, multiple voids will form on the same grain boundaries and therefore will more easily coalesce. In our case, it appears that for the SGCu material and the short pulse that void growth is also the dominant effect but over a much narrower plane and coalescence is primarily stopped by the shortness of the pulse. For the LGCu material, there are even less voids (and a slightly lower tensile strain-rate) resulting in a lower rate reload and an overall lower peak. When the pulse lengths were extended, we observed significant coalescence of voids in both materials from the initial void structure. This potentially suggests that the effect of the total grain boundary length in the spall plane as discussed in Ref. 14 was underestimated as there would have been a coupled lowering effect due to the dispersion of the particle velocity fronts. In general it is likely therefore that while the particle velocity dispersion effects discussed within the current research are important to understand and to model, the grain boundary length in the spall planes plays a more significant role.

X. CONCLUSIONS

In these experiments, we have used spatially resolved and point velocimetry measurements in conjunction with microscopy of recovered samples to study the bulk grain size effects on quasi-Taylor wave shock loaded plate impact experiments on pure copper. The particle velocity dispersion, observed and quantified using a high spatial resolution line-VISAR, has been shown to be significant for all grain sizes, but was larger for the larger bulk grains. We were also able to show some of this variation in the larger bulk grain material through multiple "point" measurements using HetV. Here, laser spot sizes were small enough to observe a difference for the larger grain materials but would need to be smaller and repeated several times to quantify the effects to the same quality as the line-VISAR.

Whilst the bulk grain size had little effect on the initiation of spallation for either bulk grain size copper or loading profile applied, the location of induced voids and the reload wave profiles observed at the free surface were notably affected. By employing sample materials with differing bulk grain sizes but a very similar surface layer grain structure, we have been able to largely decouple the effects of particle velocity dispersion created by the mesoscale grain structures from the local grain boundary lengths in the spall plane. The voids were seen to be more axially dispersed with the large bulk grain size copper, caused by the increased roughness of wave fronts. The spall reload profiles are significantly affected by the bulk grain size through the variation of void location and growth, with a slower reload signal for the larger bulk grain material.

From the results presented herein, it is clear that bulk grain size plays an important role in the development of shocks and damage in real materials. Application of models in hydrocode simulations where material structure, particle velocity dispersion, and/or the resultant effects on damage layer topography are not accounted for cannot provide a true representation of physical reality. Here we have quantified some of these effects using high resolution line-VISAR to enable continued development of mesoscale modelling. Further research will be necessary to continue this work, particularly focussing on the development of the particle velocity dispersion through different target thicknesses and grain sizes but also by application to complementary materials, such as bcc tantalum which, with a lower elastic anisotropy, might be expected to produce a lower degree of particle velocity dispersion.

ACKNOWLEDGMENTS

The authors would like to acknowledge the significant work of M. K. Philpott (AWE) in the development of the line-VISAR analysis methodology applied in this research. We would also like to thank C. Poulter, N. Bond, and S. Case (AWE), S. Johnson (formerly of Institute of Shock Physics, Imperial College London, now of AWE), and D. Pittman (Institute of Shock Physics, Imperial College London) for their significant efforts in the experimental undertaking and data analysis within this research.

[1]O. T. Strand, Rev. Sci. Instrum. **77**, 083018 (2006).
[2]L. M. Barker and R. E. Hollenbach, Rev. Sci. Instrum. **36**, 1617 (1965).
[3]D. D. Bloomquist and S. A. Shefield, J. Appl. Phys. **54**, 1717 (1983).
[4]W. F. Hemsing, A. R. Mathews, R. H. Warnes, and C. R. Whittemore, Proc. SPIE **1346**, 133 (1990).
[5]L. C. Chhabildas, W. M. Trott, W. D. Reinhart, J. R. Cogar, and G. A. Mann, in *Shock Compression of Condensed Matter*, edited by M. D. Furnish, N. N. Thadhani, and Y. Horie (American Institute of Physics, Melville, NY, 2001), p. 483.
[6]T. J. Vogler, W. M. Trott, W. D. Reinhart, C. S. Alexander, M. D. Furnish, M. D. Knudson, and L. C. Chhabildas, Int. J. Impact Eng. **35**, 1844–1852 (2008).
[7]T. J. Vogler and J. D. Clayton, J. Mech. Phys. Solids **56**, 297 (2008).
[8]M. D. Furnish, L. C. Chhabildas, W. D. Reinhart, W. M. Trott, and T. J. Vogler, Int. J. Plast. **25**, 587 (2009).
[9]M. D. Furnish, W. D. Reinhart, W. M. Trott, L. C. Chhabildas, and T. J. Vogler, in *Shock Compression of Condensed Matter*, edited by M. D. Furnish, M. Elert, T. P. Russell, and C. T. White (American Institute of Physics, Melville, NY, 2006), p. 615.
[10]B. H. Sencer, S. A. Maloy, and G. T. Gray III, Acta Mater. **53**, 3293 (2005).
[11]G. T. Gray III, N. K. Bourne, B. L. Henrie, and J. C. F. Millett, J. Phys. IV France **110**, 773 (2003).

[12]N. K. Bourne, *Materials in Mechanical Extremes* (Cambridge University Press, Cambridge, 2013).
[13]T. Chen, Z. X. Jiang, H. Peng, H. L. He, L. L. Wang, and Y. G. Wang, Strain **51**, 190 (2015).
[14]J. P. Escobedo, D. D. Koller, E. K. Cerreta, B. M. Patterson, C. M. Bronkhorst, C. M. Hansen, D. Tonks, and R. A. Lebensohn, J. Appl. Phys. **110**, 033513 (2011).
[15]S. Case and Y. Horie, J. Mech. Phys. Solids **55**, 589 (2007).
[16]G. T. Gray III, E. K. Cerreta, C. A. Yablinsky, L. B. Addessio, B. L. Henrie, B. H. Senser, M. Burkett, P. J. Maudlin, S. A. Maloy, C. P. Trujillo, and M. F. Lopez, *Shock Compression of Condensed Matter* (American Institute of Physics, Melville, NY, 2005).
[17]M. K. Philpott, A. George, G. Whiteman, J. De'Ath, and J. C. F. Millett, Meas. Sci. Technol. **26**, 125204 (2015).
[18]A. J. Barlow, Int. J. Numer. Methods Fluids **56**, 953 (2008).
[19]D. L. Preston, D. L. Tonks, and D. C. Wallace, J. Appl. Phys. **93**, 211 (2003).
[20]J. N. Johnson, J. Appl. Phys **52**, 2812 (1981).
[21]G. I. Kanel, J. Appl. Mech. Tech. Phys. **42**, 358 (2001).
[22]Y. I. Meshcheryakov and S. A. Atroshenko, Russ. Phys. J. **35**, 385 (1992).
[23]Y. I. Meshcheryakov, N. A. Mahutov, and S. A. Atroshenko, J. Mech. Phys. Solids **42**, 1435 (1994).
[24]Y. I. Meshcheryakov and A. K. Divakov, Sov. Phys. Tech. Phys. **30**, 348 (1985).
[25]M. G. Tomilin, Y. I. Meshcheryakov, S. A. Atroshenko, and N. I. Zhigacheva, Mol. Cryst. Liq. Cryst. Sci. Technol., Sect. A **251**, 343 (1994).
[26]M. A. Meyers and M. S. Carvalho, Mater. Sci. Eng. **24**, 131 (1976).
[27]M. A. Skotnikova, T. I. Strokina, N. A. Krylov, Y. I. Meshcheryakov, and A. K. Divakov, in *Shock Compression of Condensed Matter*, edited by M. D. Furnish, Y. M. Gupta, and J. W. Forbes (American Institute of Physics, Melville, NY, 2003), p. 609.
[28]J. Buchar, M. Elices, and R. Cortez, J. Phys. IV France **01**, C3-623–C3-630 (1991).
[29]R. W. Minich, J. U. Cazamias, M. Kumar, and A. J. Schwartz, Metall. Mater. Trans. A **35A**, 2663 (2004).
[30]W. R. Thissell, A. K. Zurek, D. A. S. Macdougall, D. Miller, R. Everett, A. Geltmacher, R. Brooks, and D. Tonks, AIP Conf. Proc. **620**, 475 (2002).